Transformation process from quantum beats of miniband excitons to Bloch oscillations in a GaAs/AlAs superlattice under applied electric fields

T. Hasegawa, K. Mizoguchi,* and M. Nakayama†
Department of Applied Physics, Graduate School of Engineering, Osaka City University, 3-3-138 Sugimoto, Sumiyoshi-ku, Osaka 558-8585, Japan

(Received 5 April 2007; revised manuscript received 3 August 2007; published 19 September 2007)

We have investigated the coherent dynamics of excitonic wave packets from the viewpoint of the electric-field-induced transformation from the minibands to the Wannier-Stark (WS) localization in a GaAs (6.8 nm)/AlAs (0.9 nm) superlattice embedded in a *p-i-n* diode structure with the use of a reflection-type pump-probe technique. It is clearly confirmed that the coherent-dynamics profile changes from the quantum beat of the miniband excitons to the Bloch oscillation in the WS localization with an increase in an applied bias voltage, producing an internal electric field. The key finding is that the Bloch oscillation with the frequency of $\nu_{BO}=2eFD/h$ appears in a weak-localization regime in addition to the ordinary Bloch oscillation with $\nu_{BO}=eFD/h$ in a strong-localization regime, where F is the electric field and D is the superlattice period. The experimental results of the coherent dynamics are reasonably explained by the electric-field-strength dependence of the excitonic-transition energies observed by electroreflectance spectroscopy and that of the localization profiles of the envelope functions of the electron and hole states calculated by a transfer-matrix method.

DOI: 10.1103/PhysRevB.76.115323 PACS number(s): 73.21.Cd, 78.67.Pt, 78.47.+p, 73.20.Fz

I. INTRODUCTION

Bloch oscillations (BO's) of wave packets in superlattices (SL's) have attracted much attention in physics and generation of tunable terahertz electromagnetic radiation.[1–6] The BO is a coherent dynamical process of wave packets of the Wannier-Stark (WS) localization states generated by incidence of ultrashort laser pulses. In the WS localization,[7–10] the miniband splits into a series of equally separated energy states, the so-called Stark-ladder states with an energy spacing of eFD, where F is an applied electric field along the growth direction of the SL and D is a SL period. The energies of the interband Stark-ladder transitions are given by E_0+meFD $(m=0,\pm1,\pm2,\cdots)$, where E_0 is an interband transition energy within an individual quantum well (QW) and m as an integer is a Stark-ladder index indicating an oblique transition in real space. An ultrashort laser pulse with a broad spectral width produces the coherent superposition of different Stark-ladder transitions, which results in the generation of dynamical wave packets. The wave packets spatially oscillate with a given frequency, $\nu_{BO}=eFD/h$, along the growth direction of the SL, the so-called BO. The BO frequency corresponds to the frequency of the quantum beat (QB) between the WS-localization states in the first-nearest-neighbor QW's. A theoretical research on the BO predicts that the time evolution of the oscillating wave packets strongly depends on the density weight of the envelope functions simultaneously excited by a pump light pulse.[11] On the basis of the first-nearest-neighbor tight-binding model for the WS localization,[7] the probability density of the localized envelope function in the mth-nearest-neighbor QW, P_m, is given by the following Bessel-function form:

$$P_m = J_m^2[\Delta/eFD], \tag{1}$$

where J_m is the Bessel function with an integer index m and Δ is one-half of the total energy width of the relevant miniband. According to Eq. (1), it is noted that the localization behavior of the envelope function is not gradually enhanced with an increase in electric field, but exhibits oscillatory profiles as shown in Fig. 1, where the calculated results show the probability density P_m of the envelope functions of the first quantized $(n=1)$ electron state for $m=0$, ±1, ±2 as a function of electric-field strength in a GaAs (6.4 nm)/AlAs (0.9 nm) SL that corresponds to the sample used in this work. The localization properties of the envelope functions produce complex changes of the oscillator strengths of the interband Stark-ladder transitions with a change of electric-field strength. This electric-field-strength dependence of the oscillator strength was experimentally demonstrated by using an electroreflectance (ER) spectroscopy.[12,13] Although it is expected that the BO behavior as a function of electric-field strength is also affected by the complex WS-localization characteristics, there has been no report on the BO properties from such a viewpoint. For example, if the probability density of the envelope function in the second-nearest-neighbor QW is larger than that in the first-nearest-neighbor QW, we

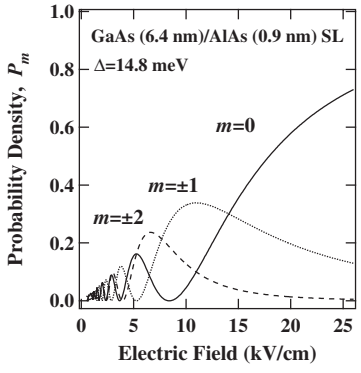

FIG. 1. Calculated results of the probability density P_m of the envelope functions for $m=0$, ±1, ±2 of the $n=1$ electron state as a function of electric-field strength using Eq. (1) in a GaAs (6.4 nm)/AlAs (0.9 nm) SL.

can expect the appearance of the BO with the frequency of $\nu_{BO}=2eFD/h$ instead of the usually observed frequency of $\nu_{BO}=eFD/h$. In Ref. 4, the possibility of appearance of such an unusual BO was suggested; however, no clear evidence for the relevant phenomenon was presented.

In this work, we have investigated the coherent dynamics of the Bloch oscillating wave packets from the viewpoint of the localization properties of the WS-localization states as described above in a GaAs (6.8 nm)/AlAs (0.9 nm) SL with a reflection-type pump-probe (PP) technique. In order to clarify the transformation process from the miniband to the WS-localization states, which reflects the localization properties of the envelope functions, we measured the applied-bias-voltage (electric-field-strength) dependence of the interband optical transitions in this SL with the use of ER spectroscopy and photocurrent (PC) spectroscopy. In addition, we calculated the electric-field-strength dependence of the envelope functions of the WS-localization states with a transfer-matrix (TM) method in the framework of an effective-mass approximation. The systematic results of the PP measurements as a function of applied bias voltage provide the observation of the transformation process from the QB between the heavy-hole (HH) and light-hole (LH) excitons under the miniband condition to the BO's in the WS localization. The key finding is that the BO with the frequency of $\nu_{BO}=2eFD/h$ is clearly observed in a weak-localization regime, and then its frequency shifts to usually observed $\nu_{BO}=eFD/h$. This fact is discussed from the experimental and theoretical results of the electric-field-strength dependence of the localization profiles of the envelope functions.

II. EXPERIMENTS

The sample used in this work was grown on an n-type (001) GaAs substrate by molecular-beam epitaxy. The SL consists of 100 periods of undoped GaAs (6.8 nm)/AlAs (0.9 nm) and is placed in the center of a p-i-n diode structure, where the n layer is a Si-doped $Al_{0.4}Ga_{0.6}As$ with a thickness of $\sim 1.0\ \mu$m and the p layer is a Be-doped $Al_{0.4}Ga_{0.6}As$ with a thickness of $\sim 0.2\ \mu$m, where the doping concentrations of Si and Be are $\sim 5\times 10^{17}$ and $\sim 1\times 10^{18}$ cm^{-3}, respectively. In addition, undoped $Al_{0.4}Ga_{0.6}As$ layers with a thickness of $\sim$50 nm were placed on both sides of the undoped SL. A heavily doped p-type GaAs cap layer with a thickness of $\sim$10 nm was finally grown for Ohmic contact. The sample was processed into a mesa structure with a size of 1.0×1.0 mm^2, and a gold-film electrode having a light window (0.7×0.7 mm^2) was formed on the surface.

The signals of the QB and BO were measured by a reflection-type PP technique. The laser source was a mode-locked Ti:sapphire pulse laser with a pulse duration of $\sim$70 fs and a repetition rate of 80 MHz. The pump and probe beams were orthogonally polarized to each other, which results in elimination of the pump-beam contribution to the probe beam. The pump light was focused onto the sample surface with a spot diameter of $\sim$0.2 mm. The pump power was kept at $\sim$3.0 mW ($\sim$120 nJ/cm^2) in order to reduce the Coulomb screening of the internal electric field by photogenerated carriers. In ER measurements, the probe light was produced by combination of a halogen lamp and a single monochromator with a spectral resolution of 0.5 nm. The applied bias was modulated with an amplitude of 100 mV and a frequency of 450 Hz around a given dc bias. The modulated reflectance signal was detected with a conventional lock-in technique. In measurements of PC spectra, PC signals were detected with a picoammeter. We simultaneously measured ER and PC spectra at various applied bias voltages. The electric-field strength was characterized by $F=(V_b-V_a)/L_i$, where V_b is the built-in voltage due to the p-n junction that is 0.9 V in the present case, V_a is the applied bias voltage, and L_i is the total length of the undoped layers. The sample temperature was kept at 10 K in all the optical measurements utilizing a closed-cycle helium cryostat.

III. RESULTS AND DISCUSSION

First, we describe the calculated results of the WS-localization states by using a TM method and the experimental results of ER spectra as a function of electric-field strength in order to clarify the electric-field-strength dependence of the eigenstates in the SL. In the TM calculation, the SL is approximated by a system of QW's with a steplike potential including an electrostatic potential having an average value of each constituent layer. This method enables us to calculate the eigenstates even at the flatband (0 kV/cm).[13,14] It is noted that Airy function, which has been usually used for the TM calculation, cannot be applied to calculate the eigenstates under almost flatband conditions because of its divergence characteristics. In this TM calculation, we used the band parameters including the band nonparabolicity according to Refs. 13 and 15. The modeled SL consists of 13 sets of GaAs (6.4 nm)/AlAs (0.9 nm) with edge layers of $Al_{0.4}Ga_{0.6}As$ for the calculations of the optical transition energies and the envelope functions of the electron and HH states. The GaAs-layer thickness was slightly changed from the designed value (6.8 nm) in the sample growth for adjusting the calculated transition energies to the observed results.

Figure 2 shows the squared overlap integral of the envelope functions of the electron and HH states in the WS-localization regime, where the notation of $I[\mathrm{E1}(\pm m)-\mathrm{HH1}(0)]$ indicates the squared overlap integral of the $n=1$ electron and HH states, m is the distance in units of SL period from the center QW with $m=0$, and the sign of $+$ $(-)$ indicates the QW in the higher (lower) potential side. The squared overlap integral shown in Fig. 2 mainly reflects the probability density of the envelope function of the $n=1$ electron in the mth-nearest-neighbor QW because the envelope function of the HH state tends to be localized in the electric-field-strength region lower than 5 kV/cm owing to the fact that the effective mass of the HH is much heavier than that of the electron. Here, we assume that the squared overlap integral corresponds to the transition probability of the relevant Stark-ladder transition.[11] Thus, it is considered that the transition probability is dominated by the localization degree of the envelope function of the electron state. In Fig. 2, the values of $I[\mathrm{E1}(0)-\mathrm{HH1}(0)]$ and $I[\mathrm{E1}(-1)-\mathrm{HH1}(0)]$ are

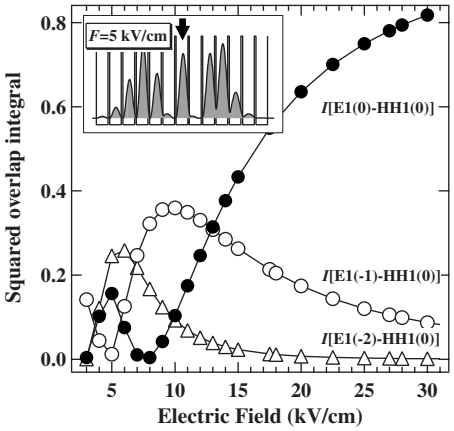

FIG. 2. Calculated results of the squared overlap integral of the envelope functions of the E1 ($\pm m$) and HH1(0) states as a function of electric-field strength in the modeled GaAs (6.4 nm)/AlAs (0.9 nm) SL with the use of the TM method. The inset shows the calculated result of the squared envelope function of the $n=1$ electron state belonging to the QW indicated by the arrow at 5 kV/cm.

dominant at $F \geqslant \sim 10$ kV/cm. This result suggests that the Stark-ladder transitions with $m=0$ and -1 are dominantly excited at $F \geqslant \sim 10$ kV/cm. This leads to the generation of the BO with the usual frequency of eFD/h. On the other hand, in the electric-field-strength region lower than ~ 10 kV/cm, the value of $I[\mathrm{E1}(-2)-\mathrm{HH1}(0)]$ is considerable. Furthermore, the value of $I[\mathrm{E1}(-2)-\mathrm{HH1}(0)]$ is larger than that of $I[\mathrm{E1}(-1)-\mathrm{HH1}(0)]$ around $F=6$ kV/cm. The inset in Fig. 2 shows the calculated result of the squared envelope function of the E1(0) state at 5 kV/cm. It is obvious that the probability density of the envelope function in the first-nearest-neighbor QW is much smaller than that in the center and second-nearest-neighbor QW's. In this situation, we can selectively excite the interband Stark-ladder transitions with $m=0$ and -2, which leads to the quantum interference between the E1(0) and E1(-2) states; namely, the BO with the unusual frequency of $2eFD/h$ occurs, which has not been observed until now. This is the key point in the present work.

Figure 3 shows the image map of the ER spectra of the interband Stark-ladder transitions as a function of applied bias voltage, where the electric-field strength is indicated on the top axis. In Fig. 3, the ER intensity is represented by the gray scale shown on the right side, and the energies of the HH and LH transitions related to the $n=1$ quantized states, which are labeled H11 and L11, calculated by the TM method are indicated by the solid and dashed curves, respectively, where the number in parentheses indicates the Stark-ladder index. The arrows belonging to the labels of H11(Γ) and L11(Γ) on the left side indicate the transition energies of the H11 and L11 transitions at the Γ point in the miniband dispersion calculated by the well-established Kronig-Penney model in the framework of the effective-mass approximation. It is noted that the applied-bias-voltage (electric-field-strength) dependence of the observed transition energies drastically changes at ~ 0.5 V (~ 5 kV/cm) for the H11 transition and at ~ 0.3 V (~ 7 kV/cm) for the L11 transition;

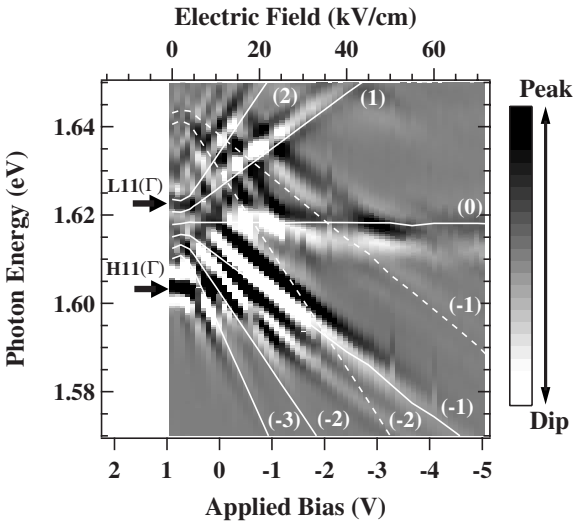

FIG. 3. Image map of the ER spectra of the interband transitions as a function of applied bias voltage in the GaAs (6.8 nm)/AlAs (0.9 nm) SL at 10 K, where the ER intensity is represented by the gray scale shown on the right side. The solid and dashed curves indicate the energies of the H11 and L11 transitions, respectively, calculated by the TM method.

namely, the Stark-ladder transitions appear with a further increase in reverse bias voltage. In Fig. 3, the ER signals related to the H11(m) transitions with $m=0$, -1, and -2 are clearly observed in the WS-localization regime. In PP measurements, we adjusted the pump energy at 1.600 eV, where the full width at half maximum (FWHM) of the pump light is ~ 30 meV. The energy position of this pump light can excite simultaneously the H11(Γ) and L11(Γ) transitions under the miniband condition and the H11(m) transitions with $m=0$, -1, and -2 in the WS-localization regime.

Figure 4 shows the time-resolved reflectivity changes at various applied bias voltages, where the thick curves indicate the numerically extracted oscillatory signals. It is noted that the period and amplitude of the observed oscillatory signal markedly change with an increase in reverse bias voltage (electric-field strength). In addition, the shape of the initial part around 0 ps of the time-resolved reflectivity change, which presumably arises from many-body effects of the electronic system,[16] clearly changes in $V_a \leqslant -1.0$ V. This change of the initial shape may reflect the transformation process from the miniband to the WS-localization state by electric field according to the bias-voltage dependence of ER spectra shown in Fig. 3.

Figure 5 shows (a) the time-domain oscillatory signals extracted from the time-resolved reflectivity changes at various bias voltages with a step of 0.1 V and (b) the Fourier-transform (FT) spectra of the oscillatory signals in Fig. 5(a). In Fig. 5, we can roughly classify the oscillation profiles to the following two regimes. In the applied-bias-voltage range from 0.6 to -0.8 V, the period and frequency of the oscillatory signal are almost constant, while those clearly exhibit the bias-voltage dependence in $V_a \leqslant -0.8$ V corresponding to a higher electric field range. We note that an effective electric-field strength inside the SL cannot be simply esti-

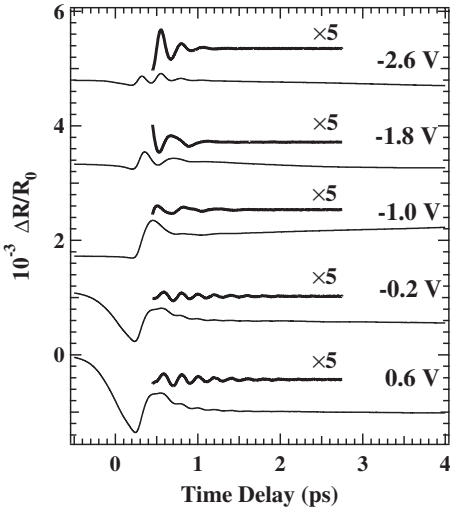

FIG. 4. Time-resolved reflectivity changes at various applied bias voltages in the GaAs (6.8 nm)/AlAs (0.9 nm) SL at 10 K, where the thick curves indicate the numerically extracted oscillatory signals.

mated from the bias voltage because of Coulomb screening by photogenerated carriers. In the lower electric field range, the observed constant frequency of ~4.9 THz almost agrees with the expected value (~4.8 THz) of the QB between the

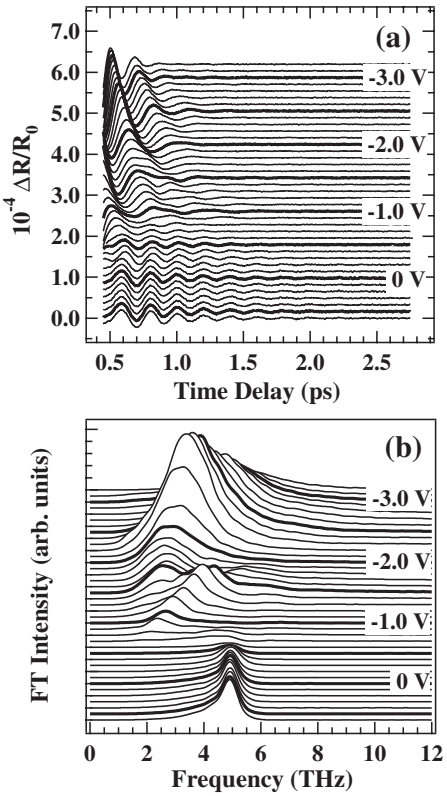

FIG. 5. (a) Time-resolved oscillatory signals extracted from the time-resolved reflectivity changes as a function of applied bias voltage with a step of 0.1 V in the GaAs (6.8 nm)/AlAs (0.9 nm) SL at 10 K. (b) FT spectra of the time-domain oscillatory signals shown in (a).

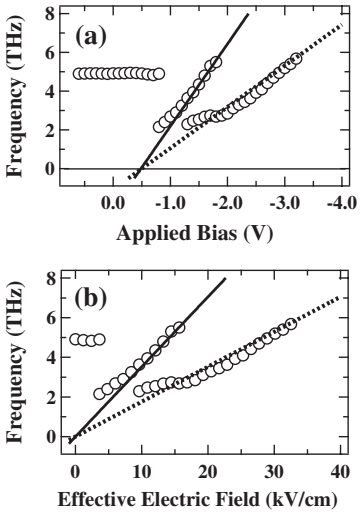

FIG. 6. (a) Peak frequencies of the FT spectra as a function of applied bias voltage. (b) Peak frequencies of the FT spectra as a function of effective electric-field strength, where the effective electric-field strength is calculated as $F_e=[(V_b-V_a)-1.4)]/L_i$. The solid and dashed lines indicate $2eF_eD/h$ and eF_eD/h, respectively.

HH and LH excitons at the Γ point in the miniband dispersion estimated from the ER spectrum under the flatband condition. Thus, the coherent oscillation in the lower electric field range is due to the QB of the miniband excitons. So, the disappearance of this QB indicates that the electronic state is transformed from the miniband to the WS-localization state. Therefore, the oscillatory signals observed in the higher electric field range are attributed to the BO in the WS-localization regime. The important finding is the fact that two types of FT peak obviously appear in the WS-localization regime. It seems that this behavior reflects the complex localization profiles of the electron envelope functions described above with Fig. 2; namely, the BO with the frequency of $2eFD/h$ appears in a weak-localization regime, and then the usual BO with eFD/h occurs in a strong-localization regime.

In order to quantitatively analyze the properties of the BO, we have to estimate an effective electric-field strength, taking account of the Coulomb screening effect. Figure 6(a) shows the peak frequencies of the FT spectra as a function of applied bias voltage. In Fig. 6(a), we notice two kinds of bias-voltage dependence of the peak frequency in addition to the constant frequency of ~4.9 THz corresponding to the QB of the miniband excitons. Here, we assume on the basis of the WS-localization characteristics described above that the steep dependence and gentle dependence on the bias voltage are attributed to the BO's with the frequencies of $2eF_eD/h$ and eF_eD/h represented by the solid and dashed lines, respectively, where F_e is the effective electric field given by $F_e=[(V_b-V_a)-1.4]/L_i$. The offset value of 1.4 V phenomenologically means an effect of the Coulomb screening on the internal electric field by accumulated carriers at the interfaces between the SL and clad layers.[4] Figure 6(b) shows the peak frequencies as a function of effective electric-field strength: $2eF_eD/h$ (solid line) and eF_eD/h (dashed line). The slopes of the solid and dashed lines well

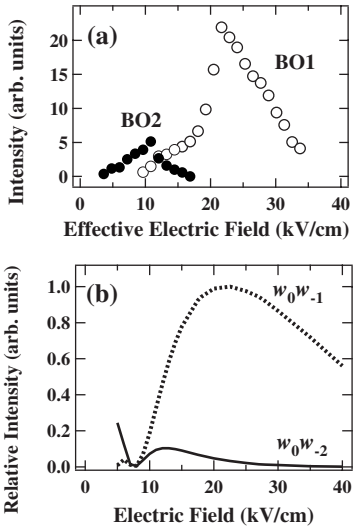

FIG. 7. (a) Integrated intensities of the FT spectra as a function of effective electric-field strength. (b) Calculated results of the product of the spectral weights, w_0w_{-1} and w_0w_{-2}, as a function of electric-field strength.

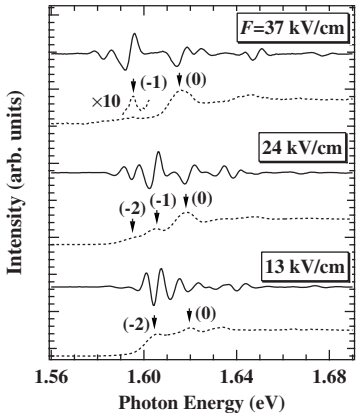

FIG. 8. ER and PC spectra at various electric-field strengths in the GaAs (6.8 nm)/AlAs (0.9 nm) SL at 10 K, where the PC spectra are represented by the dashed curves. The arrows indicate the energies of the PC peaks, and the number in parentheses means the Stark-ladder index of the H11 transition.

explain the peak frequencies. This fact indicates that the estimation of F_e is reasonable.

In Fig. 6(b), it is obvious that the QB of the miniband excitons disappears at F_e=4 kV/cm. This electric-field strength is almost consistent with that (~5 kV/cm) at which the ER signal related to the H11(Γ) transition in the miniband regime disappears, as shown in Fig. 3. This also supports the appropriateness of the estimation of F_e. At F_e =4 kV/cm, the unusual BO with the frequency of $2eFD/h$, which results from the quantum interference between the H11(0) and H11(−2) excitons, occurs. Subsequently, the usual BO with the frequency of eFD/h begins to appear at F_e=10 kV/cm. Hereafter, we call the BO's with the frequencies of $2eFD/h$ and eFD/h by BO2 and BO1, respectively. This transformation of the BO profile with an increase in electric-field strength is due to the enhancement of the WS localization. BO1 and BO2 coexist in the electric-field-strength range from 10 to 15 kV/cm, which is consistent with the simultaneous observation of the Stark-ladder transitions with m=−2 and −1, as shown in Fig. 3. In Fig. 6(b), several experimental frequencies slightly deviate from the slopes of $2eF_eD/h$ and eF_eD/h. This deviation may be due to some inhomogeneity of the internal electric field.

Finally, we discuss the intensities of BO1 and BO2. Figure 7(a) shows the integrated intensity of the FT spectra related to BO1 and BO2 as a function of effective electric-field strength. In Fig. 7(a), the electric-field strength at which the BO1 (BO2) intensity reaches a maximum is 22(11) kV/cm. In order to analyze the experimental results, we consider a three-level system describing a ground state, $|0\rangle$, and two excited states, $|\mathrm{H11}(0)\rangle$ and $|\mathrm{H11}(m)\rangle$ (m=−1 or −2). In the three-level-system description, the intensity of the PP signal related to the BO can be represented by the following equation:[17]

$$I_{\mathrm{BO}} \propto w_0^2 + w_m^2 + w_0 w_m[1 + \cos(\Delta E t)e^{-\gamma t}], \qquad (2)$$

where w is a spectral weight of the optical transition, ΔE and γ indicate an energy spacing and a phase relaxation rate between the simultaneously excited states, respectively, and the subscript m means the Stark-ladder index. The spectral weight w is defined by the product of $S_{\mathrm{pump}}[E_m(F)]$ and $T[E_m(F)]$, where $S_{\mathrm{pump}}[E_m(F)]$ is an electric-field amplitude of the pump light at the Stark-ladder transition energy of $E_m(F)$ depending on the electric-field strength F and $T[E_m(F)]$ is a transition probability. From Eq. (2), it is evident that the intensity of the BO is determined by w_0w_m.

In the calculation of $S_{\mathrm{pump}}[E_m(F)]$, $E_m(F)$ is obtained from the electric-field-strength dependence of the ER spectra shown in Fig. 3. For the estimation of the precise transition energy from the ER signal, it is necessary to analyze the line shape of the ER spectra based on a dielectric function form; however, we cannot exactly determine that of the Stark-ladder transition. Here, we compare the ER and PC spectra to determine the transition energies because the PC-peak energy usually corresponds to the transition energy. Figure 8 shows the ER and PC spectra at various electric-field strengths, where the PC spectra are represented by the dashed curves. The arrows indicate the energies of the PC peaks, and the number in parentheses means the Stark-ladder index of the H11 transition. From the comparison between the ER and PC spectra, the dip energies of the H11(0) and H11(−2) ER signals correspond to the transition energies, while the peak energy of the H11(−1) signal is equivalent to the transition energy. The uncertainty of determination of the transition energy is about ±2 meV according to the linewidth in the present case. The spectrum of the pump light was approximated by the Gaussian function with a FWHM of 30 meV. In the calculation of $T[E_m(F)]$, we used the squared overlap integral shown in Fig. 2, because the value of the squared overlap integral can be attributed to the transition probability of the relevant Stark-ladder transition.

Figure 7(b) shows the calculated results of the w_0w_{-1} and w_0w_{-2} for BO1 and BO2 with the frequencies of eFD/h and $2eFD/h$, respectively, as a function of electric-field strength. The electric-field strengths at which the products of the spectral weights exhibit the maximum almost agree with those of the experimental results. In the calculation, the value of w_0w_{-2} shows the dip feature at ~8 kV/cm. This reflects the dip feature of $I[\mathrm{E1}(0)-\mathrm{HH1}(0)]$ as shown in Fig. 2; however, the dip profile is not observed in the experimental results. In addition, the calculated results more slowly vary as a function of electric-field strength in comparison with the experimental results. We discuss the difference between the experimental and theoretical results. In the present calculation, we ignore the excitonic effect, which affects the optical transition, and the inhomogeneity of the internal electric field. These factors should modify the transition probability $T[E_m(F)]$. Moreover, we also ignore the damping factor of the coherent oscillation due to a scattering process. The effect of the damping reduces the BO intensity especially at high electric-field strengths. In order to reproduce precisely the electric-field-strength dependence of the BO intensity, we have to take account of the knotty problems in theory described above, which is beyond the scope of this work. Nevertheless, the electric-field-strength dependence of the BO intensity is semiquantitatively explained by the calculation based on the simple model used here.

IV. CONCLUSIONS

We have investigated the coherent dynamics of the excitonic wave packets from the viewpoint of the transformation process from the miniband to the WS-localization state in the GaAs (6.8 nm)/AlAs (0.9 nm) SL with the reflection-type PP technique at 10 K together using the energy spectra obtained by ER spectroscopy. We have found that the unusual BO (BO2) with the frequency of $2eFD/h$ occurs just after the disappearance of the QB of the miniband excitons. Subsequently, the usual BO (BO1) with the frequency of eFD/h becomes dominant with a further increase in electric-field strength. The electric-field-strength dependence of the BO1 and BO2 intensities is semiquantitatively explained on the basis of the simple three-level-system model taking account of the electric-field-strength dependence of the Stark-ladder transition energies measured with ER spectroscopy and that of the squared overlap integral of the envelope functions of the electron and hole states calculated by the TM method. Thus, we provide a different aspect of the BO.

ACKNOWLEDGMENT

This work was partially supported by the Grant-in-Aid for Scientific Research, No. 18340090, from Japan Society for the Promotion of Science.

*Present address: Department of Physical Science, Graduate School of Science, Osaka Prefecture University, Gakuen, Naka-ku, Sakai, Osaka 599-8531, Japan.

†nakayama@a-phys.eng.osaka-cu.ac.jp

[1] J. Feldmann, K. Leo, J. Shah, D. A. B. Miller, J. E. Cunningham, T. Meier, G. von Plessen, A. Schulze, P. Thomas, and S. Schmitt-Rink, Phys. Rev. B **46**, 7252 (1992).

[2] K. Leo, P. Haring Bolivar, F. Brüggemann, R. Schwedler, and K. Köhler, Solid State Commun. **84**, 943 (1992).

[3] C. Waschke, H. G. Roskos, R. Schwedler, K. Leo, H. Kurz, and K. Köhler, Phys. Rev. Lett. **70**, 3319 (1993).

[4] P. Leisching, P. Haring Bolivar, W. Beck, Y. Dhaibi, F. Brüggemann, R. Schwedler, H. Kurz, K. Leo, and K. Köhler, Phys. Rev. B **50**, 14389 (1994).

[5] T. Dekorsy, R. Ott, H. Kurz, and K. Köhler, Phys. Rev. B **51**, 17275 (1995).

[6] For a review, K. Leo, *High-Field Transport in Semiconductor Superlattices* (Springer, Berlin, 2003), and references for the Bloch oscillations therein.

[7] J. Bleuse, G. Bastard, and P. Voisin, Phys. Rev. Lett. **60**, 220 (1988).

[8] E. E. Mendez, F. Agulló-Rueda, and J. M. Hong, Phys. Rev. Lett. **60**, 2426 (1988).

[9] P. Voisin, J. Bleuse, C. Bouche, S. Gaillard, C. Alibert, and A. Regreny, Phys. Rev. Lett. **61**, 1639 (1988).

[10] For a review, M. Nakayama, *Optical Properties of Low-Dimensional Materials* (World Scientific, Singapore, 1995), Chap. 3, p. 197, and references for the Wannier-Stark localization therein.

[11] M. Dignam, J. E. Sipe, and J. Shah, Phys. Rev. B **49**, 10502 (1994).

[12] I. Tanaka, M. Nakayama, H. Nishimura, K. Kawashima, and K. Fujiwara, Solid State Commun. **92**, 385 (1994).

[13] T. Hasegawa and M. Nakayama, Jpn. J. Appl. Phys., Part 1 **44**, 8340 (2005).

[14] I. Tanaka, M. Nakayama, H. Nishimura, K. Kawashima, and K. Fujiwara, Phys. Rev. B **48**, 2787 (1993).

[15] D. F. Nelson, R. C. Miller, C. W. Tu, and S. K. Sputz, Phys. Rev. B **36**, 8063 (1987).

[16] G. Bartels, G. C. Cho, T. Dekorsy, H. Kurz, A. Stahl, and K. Köhler, Phys. Rev. B **55**, 16404 (1997).

[17] K. Leo, J. Shah, E. O. Göbel, T. C. Damen, S. Schmitt-Rink, W. Schäfer, and K. Köhler, Phys. Rev. Lett. **66**, 201 (1991).